Chapter 5

Development of Optical Waveguides Through Multiple-Energy Ion Implantations

Heriberto Márquez Becerra, Gloria V. Vázquez, Eder G. Lizárraga-Medina, Raúl Rangel-Rojo, David Salazar and Alicia Oliver

Additional information is available at the end of the chapter

http://dx.doi.org/10.5772/67829

Abstract

In this chapter, we present information about the design, fabrication and characterization of optical waveguides obtained by using a protocol of multiple energy ion implantations. This protocol must provide an approach to produce optical waveguides with adequate features, such as dimensions, evanescent field and optical confinement. In general, optical waveguides can be improved by widening the optical barrier or waveguide core through multiple energy ion implantations. Design of optical waveguides must consider effects induced by the ion implantation process, such as modification of substrate density, polarizability and structure. Information will be presented about optical waveguides formed mainly in laser crystals (i.e., Nd:YAG, Nd:YVO_4) using light ions such as H and He+ and heavy ions such as C_2+. In general, these ions decrease the refractive index in the implanted area, producing a barrier that permits guiding in the region near the surface. Furthermore, information about nonlinear optical properties of channel waveguides containing metallic nanoparticles is presented. Composite materials containing metallic nanoparticles embedded in a dielectric matrix such as silica possess interesting properties due to surface plasmon resonance absorption features and the enhancement of the third-order nonlinear optical response. Therefore, nonlinear optical properties in composite waveguides can be used in all-optical switching devices.

Keywords: optical waveguides, multi-energy ion implantation

1. Introduction

Since the 1960s, waveguide optics has evolved into an emerging discipline and has a tremendous impact on our information society, due to the potential applications for signal processing

and biochemical sensing [1]. The first proton implantation in fused silica to form waveguides was reported in 1968 [2]. Then, ion-implanted waveguide progress has been reviewed by Townsend et al. summarizing early results before 1993 [3]. In recent years, Chen et al. and Liu et.al. presented review papers [4–6] showing advances from 1994 to 2013. Ion implantation has been used to produce optical waveguides in several substrates, including more than 100 materials such as single crystals, glasses, polycrystalline ceramics and organic materials. Moreover, ion implantation allows accurate control of both dopant composition and penetration depth through the choice of the species and the energy of the ions. Waveguides can be fabricated at low temperature, which ensures steady chemical compositions and phases in the waveguide region. Waveguides can be fabricated by combining ion implantation with other techniques, such as ion exchange and metal ion diffusion [7, 8].

Single ion implantation has been used as a rule to produce optical waveguides, but there is a lack of control of optical confinement that limits its potential as optical waveguides [9]. However, optical waveguides can be improved by widening the barrier or directly generating the waveguide core through multiple energy ion implantations [10, 11]. There are a few works related to optical waveguides obtained by means of multiple ion implantations [12, 13]. In this chapter, multi-energy ion implantation is used to fabricate optical waveguides.

2. Theory

2.1. Optical waveguides

The simplest optical waveguide structure is the planar or slab waveguide. It is composed of a refractive index material surrounded by two lower refractive index materials, and it confines light in one direction. **Figure 1** shows the typical three-layer configuration of a planar waveguide, where n_1 is the refractive index of the core and n_2 and n_3 are the refractive indices of substrate and cladding, respectively ($n_1 > n_2 > n_3$). Considering a plane wave travelling in a slab waveguide structure, with a dielectric square shape core refractive index, an eigenvalue equation that describes light propagation can be obtained for transverse electric (TE) and transverse

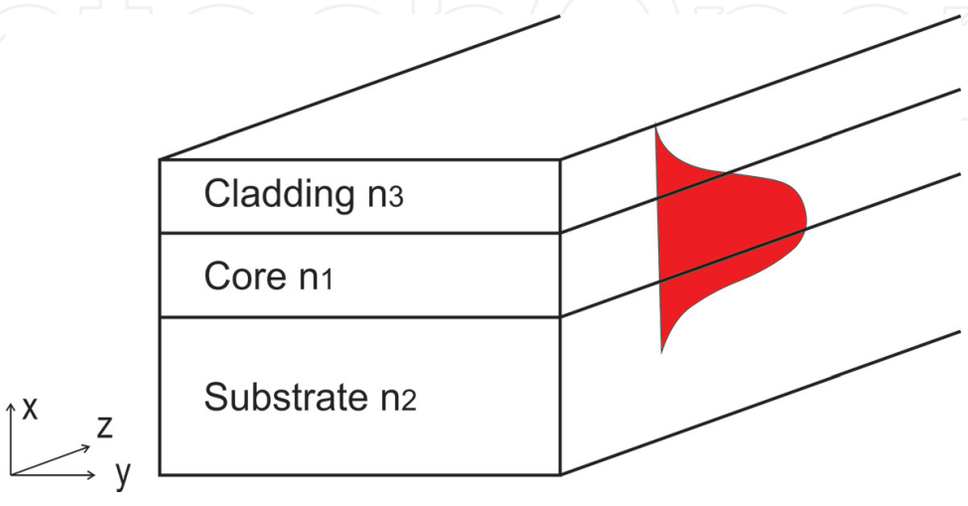

Figure 1. A three-layer configuration of a slab optical waveguide.

http://dx.doi.org/10.5772/67829

magnetic (TM) wave polarizations, Eqs. (1) and (2), for a three-layer dielectric waveguide structure [14]:

$$k_a a = tan^{-1}\frac{k_c}{k_a} + tan^{-1}\frac{k_s}{k_a} + m\pi \tag{1}$$

$$k_a a = \frac{1}{d}tan^{-1}\frac{k_c}{k_a} + \frac{1}{c}tan^{-1}\frac{k_s}{k_a} + m\pi \tag{2}$$

where a is the film physical thickness, $k_a = k\sqrt{n_a^2 - n_e^2}$, $k_s = k\sqrt{n_e^2 - n_s^2}$, and $k_c = k\sqrt{n_e^2 - n_c^2}$ are the transversal wavenumbers in the core, substrate, and cladding, respectively, and $k = 2\pi/\lambda$ is the wavenumber; $c = n_s^2/n_a^2$ and $d = n_c^2/n_a^2$ are parameters introduced in the TM eigenvalue equation. Furthermore, an effective index n_e can be obtained for every integer m number; this solution is known as the m_{th} mode and has its own light distribution at the waveguide structure. The distribution of the electric field amplitude is given by:

$$E_y(x) = \begin{cases} E_c e^{-\sigma_c x}, \ x \geq 0 \\ E_c\left[\cos(\kappa_a x) - \dfrac{\sigma_c}{\kappa_a}\sin(\kappa_a x)\right], \ -a \leq x \leq 0. \\ E_c\left[\cos(\kappa_a a) - \dfrac{\sigma_c}{\kappa_a}\sin(\kappa_a a)\right] e^{\sigma_s(x+a)}. \ x \leq -a \end{cases} \tag{3}$$

The light confinement, Γ, is defined as a ratio between the light power in the core and the total mode power and is calculated from [15]:

$$\Gamma = \frac{P_{film}}{P} = \frac{1 + \frac{k_s}{k_f^2 + k_s^2} + \frac{k_c}{k_f^2 + k_c^2}}{f + \frac{1}{k_s} + \frac{1}{k_c}}. \tag{4}$$

2.2. Ion implantation process

The ion implantation has proven to be a powerful technique to fabricate optical waveguides in a variety of materials. In the case of light ions that are implanted, the damage caused by the nuclear collisions during the implantation reduces the physical density of the substrate. The low-density buried region, with refractive lower than the substrate, acts as an optical barrier. The region between the surface and the optical barrier has a higher refractive index and can operate as a waveguide [12]. By contrast, heavy ions can increase physical density, polarizability or structure of the substrate, which results in an increase in the refractive index of the implanted region surrounded by regions with lower refractive index, making a typical optical waveguide [13].

Nuclear damage processes, which create partial lattice disorder in the material, also can introduce a positive or negative change in the refractive index, depending on the ionization and diffusion effects. The index profile depth can be controlled by the ions energy, and the positive or negative change in the refractive index will allow one to have a waveguide core or an optical barrier [3]. The changes in the refractive index n mostly depend on the defect content (ΔV), changes in the polarizability ($\Delta\propto$) and structure factors (F). The Wei adaptation of the Lorentz-Lorenz equation gives [16]:

$$\frac{\Delta n}{n} = \frac{(n^2-1)(n^2+2)}{6n^2}\left[-\frac{\Delta V}{V} + \frac{\Delta \propto}{\propto} + F\right]. \tag{5}$$

When the dominant mechanism is a negative ΔV, an optical barrier will be produced beneath the substrate surface. On the other hand, a positive ΔV may lead to an increase in the refractive index acting as the core of the waveguide. Glass implanted with heavy ions such as Ag and Cu follows this behaviour. Furthermore, an annealing procedure can generate metal nanoparticles in the waveguide, which have potential as nonlinear optical devices [17].

3. Methodology and materials

The development of optical waveguides by a multi-implantation process shown in blocks in **Figure 2** requires feedback from optical design software, ion implantation simulations, optical characterization and optimization. Once specific requirements are defined for the design of optical waveguides, it is necessary to know basic information of the first approach of waveguide parameters such as Δn and core dimensions. Afterwards, it is necessary to try to replicate these features through the ion implantation process. The prediction of ion range and damage distribution is essential for the ion implantation technique and thus several computer simulation programs have been developed such as the Stopping and Range of Ions in Matter (SRIM), crystal- Transport of Ions in Matter (crystal-TRIM), Projected Range Algorithm (PRAL), MARLOWE, University of California MARLOWE (UC-MARLOWE), University of Valladolid MARLOWE (UVAMARLOWE), REED and so on [18–22]. Here, the ion trajectory was simulated by the Stopping and Range of Ions in Matter (SRIM) software [23], while the ions were implanted by the NEC Pelletron Accelerator Model 9SDH-2 at the Instituto de Física, UNAM. The experimental parameters used to fabricate SiO_2 planar waveguides by Ag+ multiple implantation process are shown in **Table 1**.

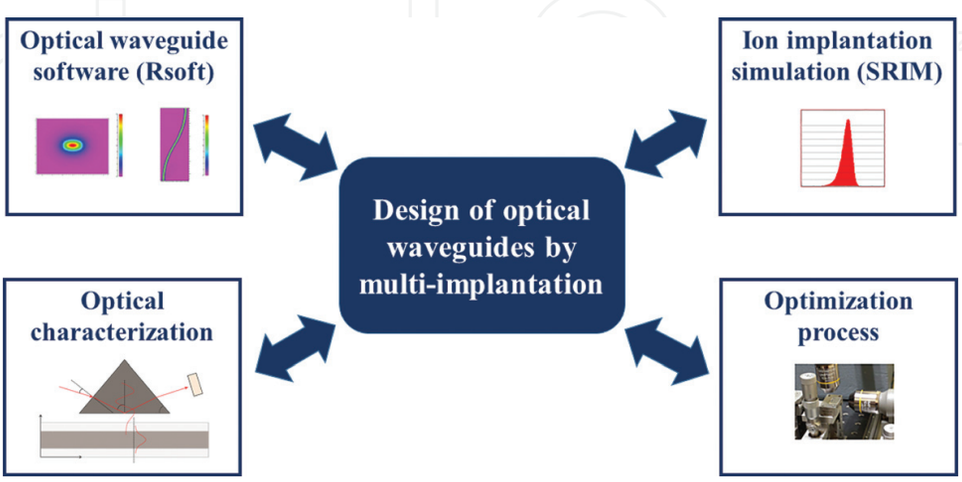

Figure 2. A diagram for the development of optical waveguides by a multi-implantation process.

http://dx.doi.org/10.5772/67829

Implant energy	Fluence [ions/cm^2]			
	M1	**M2**	**M3**	**M4**
9 MeV	5×10^{14}	1×10^{15}	2.5×10^{15}	5×10^{15}
7 MeV	2.5121×10^{14}	5.025×10^{14}	1.256×10^{15}	2.5119×10^{15}
6 MeV	1.4748×10^{14}	2.9505×10^{14}	7.3757×10^{14}	1.475×10^{15}
5.2 MeV	2.0689×10^{14}	4.1375×10^{14}	1.034×10^{14}	2.069×10^{15}
4.3 MeV	1.9508×10^{14}	3.9×10^{14}	9.75×10^{14}	1.95×10^{15}

Table 1. Parameters of implantation used for the samples M1–M4 [13].

An automatic prism-coupling system, (Metricon Model 2010) operating at a wavelength of 633 nm, was used for obtaining TE/TM effective refractive indices of the waveguides propagation modes, and propagation losses were determined by a transmission technique; both techniques are described later.

Also, results will be reviewed for the waveguides fabricated in laser crystals such as YAG and YVO_4 doped with Nd or Yb. These results deal mainly with refractive index changes and laser emission properties.

4. Results and discussions

4.1. Initial parameters for optical waveguides

The single mode of behaviour of the waveguide in the Near Infrared (NIR) was considered as a major goal. Calculations by means of the Reflectivity Calculation Method (RCM) result in a step-index waveguide with a core width of ~3 μm and index change of Δn~0.008, whose intensity mode profiles are shown in **Figure 3**.

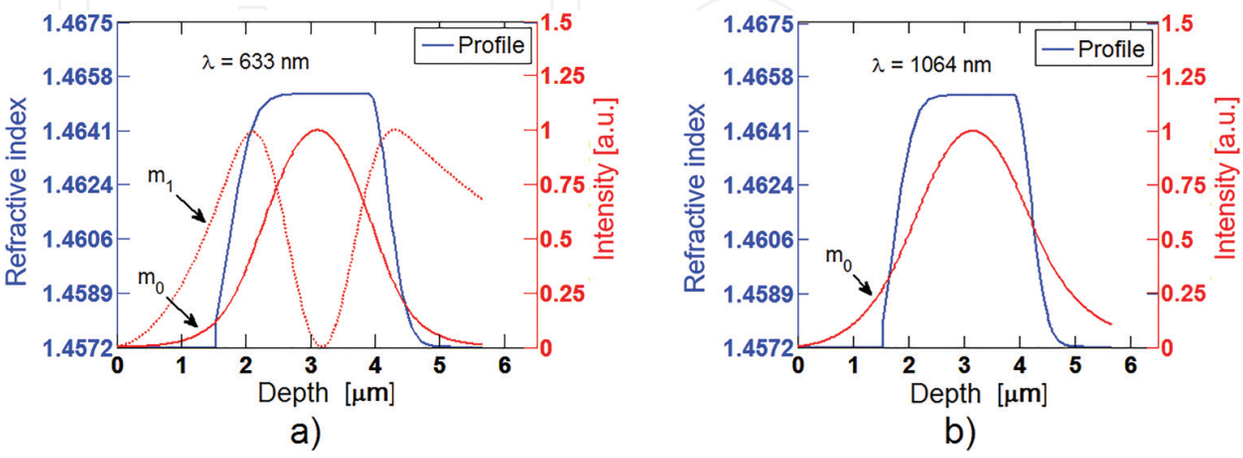

Figure 3. Intensity distribution of propagation modes confined in a step-index waveguide with refractive index change *Δn~0.008* for: (a) λ = 633 *nm* and (b) λ = 1064 *nm*.

4.2. Design of waveguides through multiple energy ion implantations

The methodology oriented to design optical waveguides in a dielectric matrix, by means of ion implantation, must consider parameters as: (a) type of ion, energy, fluence and (b) composition and structure of the substrate trying to obtain a specific waveguide. Moreover, changes in the properties of the substrate during the ion implantation, for example, structural, density or polarizability must be considered for a robust waveguide design.

4.2.1. Optical waveguides by heavy (Ag) ion implantation

First, the silver ion implantation profile was calculated using energies from 1 to 10 MeV and fluences from 10^{14} to 10^{15} ions/cm^2 in an SiO_2 substrate; see **Figure 4(a)** [17]. As an example, **Figure 4(b)** shows a step ion distribution obtained from multiple silver implantation energies and fluences: 9 MeV, 5x10^{14} ions/cm^2; 7 MeV, 2.5x10^{14} ions/cm^2; 6 MeV, 1.47x10^{14} ions/cm^2; 5.2 MeV, 2x10^{14} ions/cm^2 and 4.3 MeV, 1.95x10^{14} ions/cm^2 [13].

4.2.2. Optical waveguides by light (H, He+) ion implantation

Light ion implantation normally reduces the refractive index at the end of the ion trajectory and thus an optical waveguide is created between this low index region (so-called optical barrier) and the air next to the substrate's surface, see **Figure 5**. The refractive index is reduced mainly because of a volume expansion in the damage region, producing a lower material density. Depending on the material, the refractive index in the guiding region may increase or decrease slightly due to polarizability and structural factors, according to Eq. (5). In order to reduce light leakage through the optical barrier into the substrate (i.e., light tunnelling), generally, two or three energies close to each other are used, generating broader barriers than those obtained by a single implant [24–26]. For example, helium ion energies of 1.75, 1.6 and

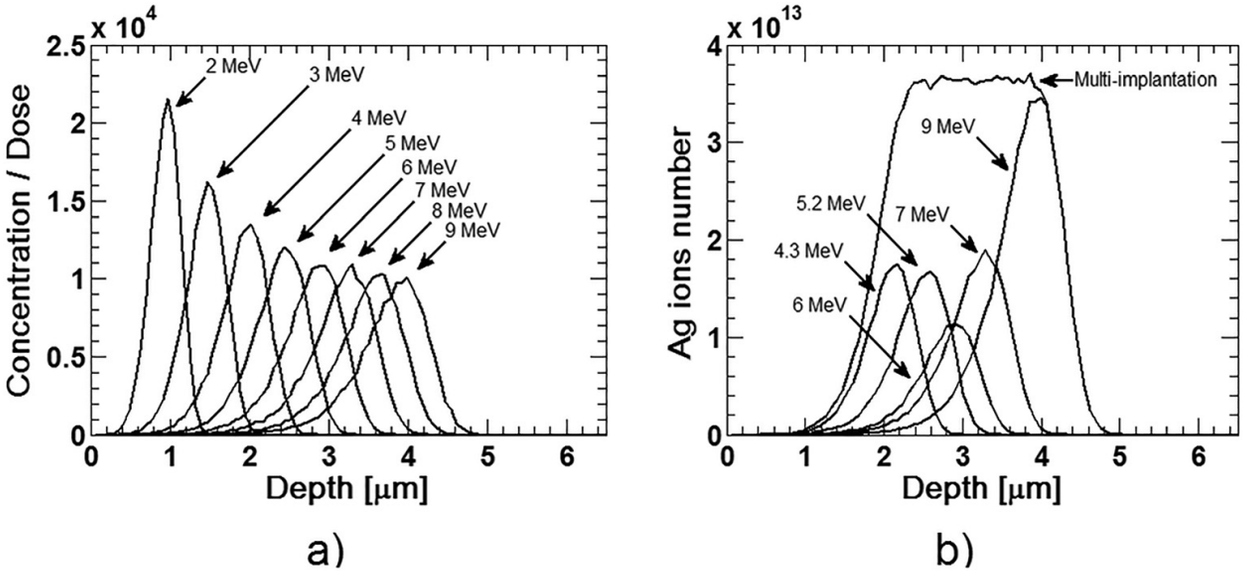

Figure 4. (a) Ag implantation profiles for a range of 2–9 MeV and (b) multiple implantations towards a generation of a step-index waveguide [13].

http://dx.doi.org/10.5772/67829

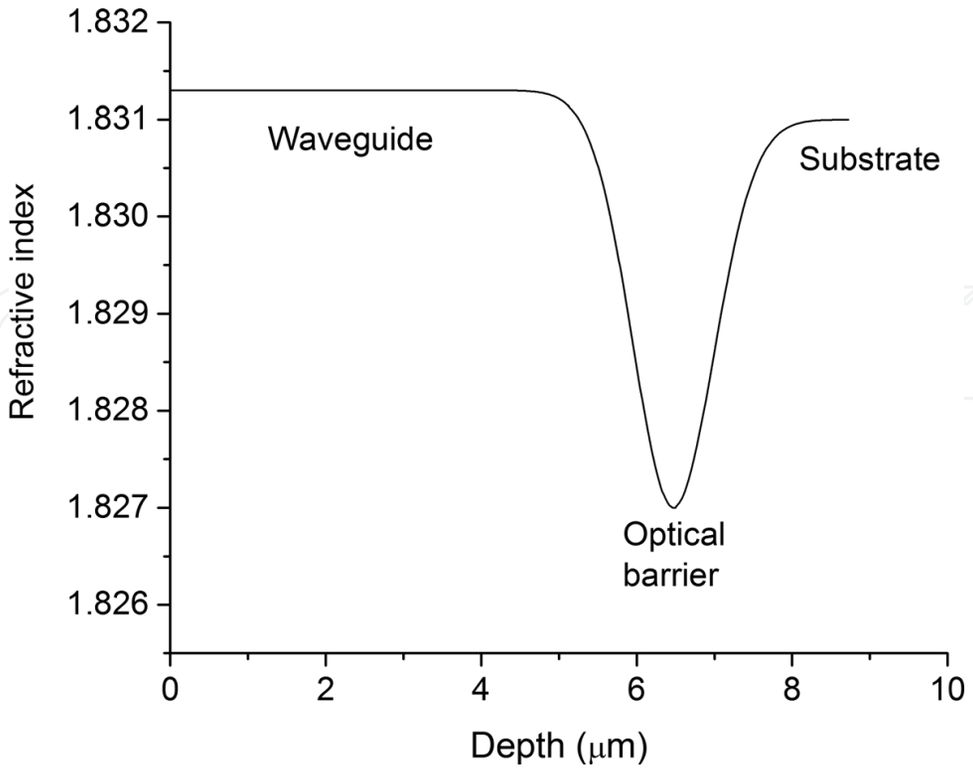

Figure 5. A refractive index profile of a Yb:YAG waveguide implanted with protons at an energy of 1 MeV and an incident angle of 46° [27].

1.5 MeV can be implanted, instead of only 1.5 MeV, at a dose of around 10^{16} ions/cm^2, reducing the tunnelling losses in the waveguide.

4.3. Passive optical waveguides

In this section, the results of optical and physical properties of ion-implanted waveguides are presented.

4.3.1. Refractive index change for an optical waveguide

One of the most important optical properties of waveguides is the refractive index change that is produced by the ion implantation process. From the complex mechanism of effects produced by ion implantation in optical materials, here, only the main contributors to the refractive index change are considered. Refractive index change is induced by the modification of the substrate density, polarizability or structure produced by radiation damage or stoichiometric changes [9–11]. An approach to analyse the refractive index change, Δn, of an ion-implanted waveguide is given by

$$\Delta n^{TE,\,TM} = \Delta n_R + \Delta n_V + \Delta n_\sigma^{TE,\,TM} \tag{6}$$

where Δn_R is mainly due to the difference in polarizability before and after ion implantation which can be calculated using a basic model that relates refractive index as a function of

chemical composition [9]. Refractive index change's contribution from volume change of the matrix surface caused by the induced compaction process, Δn_V, can be estimated across the surface implanted through AFM measurements [28]. The index change Δn_σ depends on the polarization state of the light (TE or TM) is related to the optical stress produced by ion implantation which can be determined directly using an effective index of propagation modes for TE and TM polarizations.

An initial consideration to estimate the gradient index profile of the ion implantation distribution is to calculate the ion distribution generated by the multiple ion implantation process and the corresponding refractive index. First, we calculated Δn of each segment of 70 nm of the waveguide, shown in **Figure 6(a)**. Refractive index profiles obtained for M1-M4 are shown in **Figure 6(b)**. The values of Δn_{Rmax} calculated for samples *M1-M4* are ~0.00017, ~0.00034, ~0.00089 and ~0.0017, considering a silver ion concentration of Ag_{max} ~0.04%*wt*., ~0.08%*wt*., ~0.2%*wt*. and ~0.4%*wt*., respectively.

4.3.2. Refractive index profile of optical waveguides

A way to determine the refractive index profile of an optical waveguide is by means of direct measurements of effective refractive indices of confined and radiated propagation modes using a prism-coupling technique. In the prism-coupling method, as shown in **Figure 7**, an incident light beam enters the prism at an angle φ. At the prism base, the light beam forms an angle θ to the normal. This angle, θ, determines the phase velocity in the z direction of the incident beam in the prism and in the gap between the prism and the waveguide. Efficient coupling of light into the waveguide occurs only when we choose the angle φ such that v_i is equal to the phase velocity, v_m, of one of the guided modes [29].

The effective refractive index, *Nm*, of the *m*th mode is related to θ_m, by

$$N_m = n_p sin\left[sin^{-1}\left(sin\frac{\theta_m}{n_p}\right) + A\right] \tag{7}$$

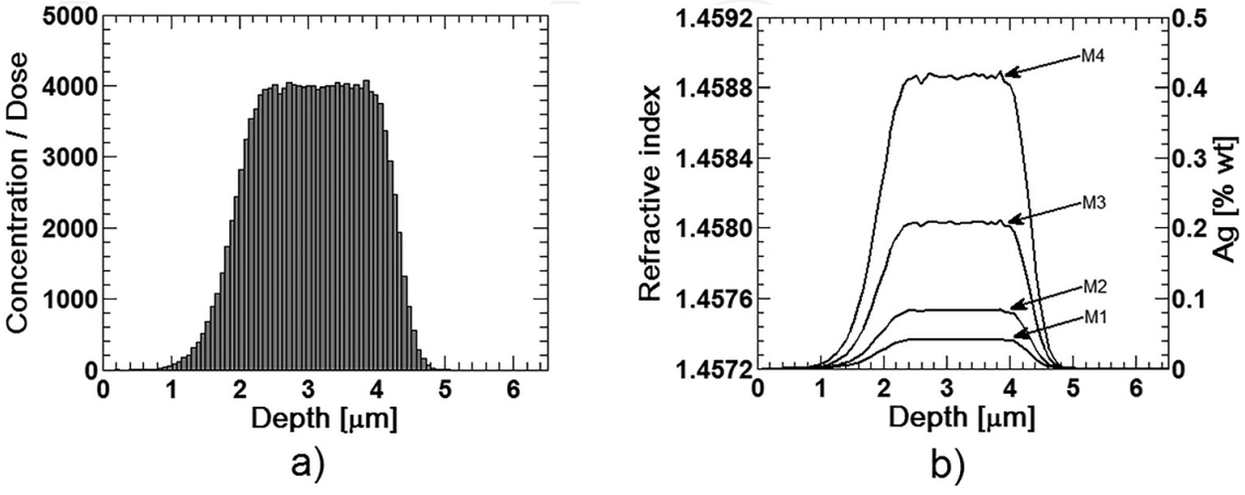

Figure 6. (a) A multiple implantation profile and (b) refractive index profiles for samples M1–M4.

http://dx.doi.org/10.5772/67829

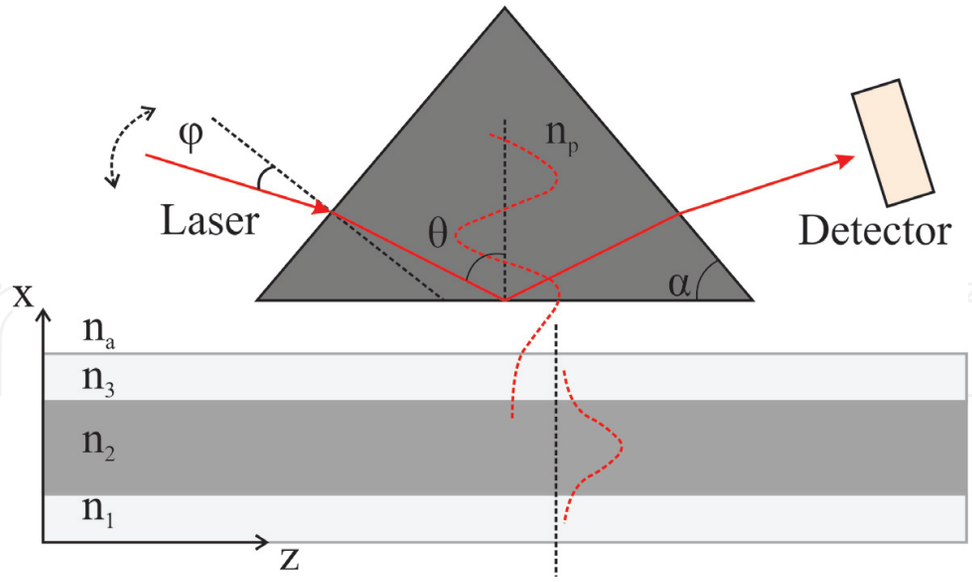

Figure 7. A principle of operation of the prism-coupling technique [29].

where A and n_p are the base angle and refractive index of the prism, respectively. The effective refractive indices of the guided modes in the SiO_2 waveguides, shown in **Table 2**, were obtained by the measurement of the coupling mode angles of the prism coupler. **Figure 8(a)** shows typical results of TE/TM effective refractive indices for the propagation modes of waveguides obtained through the prism-coupling technique. **Table 2** lists the values of TE and TM effective refractive indices for the propagation modes in the ion-implanted waveguides. Propagation modes m_0 and m_1 are guided modes and m_2, m_3 and m_4 are considered radiated modes because they do not fulfil the condition $n_3 < n_{eff} < n_2$ but are required for an adequate refractive index profile fitting [30]. Starting from a refractive index profile calculated from polarizability shown in **Figure 6(b)**, a refractive index profile for the waveguides was fitted by the RCM method for experimental and theoretical effective refractive indices of the waveguide propagation modes. Fitted refractive index profiles of waveguides, for TE/TM polarizations, are shown in **Figure 8(b)**, wherein values of refractive index from core, cladding and substrate are given, respectively.

Mode	**M1**		**M2**		**M4**	
	$\mathbf{n_{effTE}}$	$\mathbf{n_{effTM}}$	$\mathbf{n_{effTE}}$	$\mathbf{n_{effTM}}$	$\mathbf{n_{effTE}}$	$\mathbf{n_{effTM}}$
m_0	1.4640	1.4644	1.4642	1.4646	1.4640	1.4644
m_1	1.4604	1.4607	1.4607	1.4611	1.4593	1.4597
m_2	1.4542	1.4548	1.4548	1.4551	1.4518	1.4521
m_3	1.4428	1.4430	1.4431	1.4433	1.4384	1.4387
m_4	1.4275	1.4273	1.4287	1.4291	1.4192	1.4187

Table 2. Effective refractive indices of the propagation modes in the SiO_2 waveguides [13].

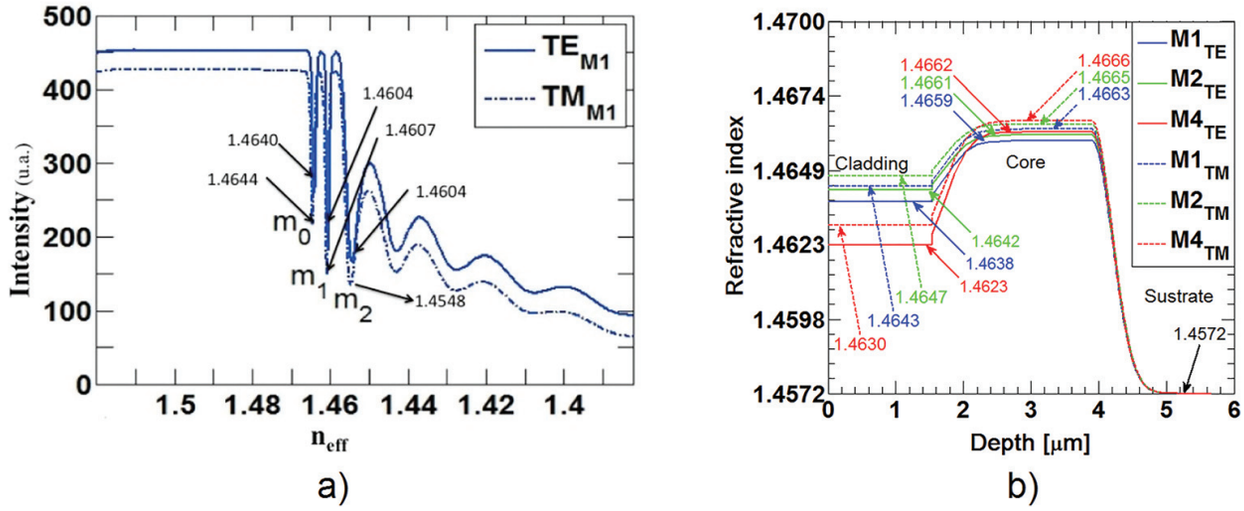

Figure 8. (a) An experimental TE/TM effective refractive index for the propagation modes of the waveguide M1 and (b) TE/TM refractive index profiles calculated for waveguides M1, M2 and M4 [13].

4.3.3. Waveguide propagation losses

Propagation losses were determined by the method of light transmission, as shown in **Figure 9**. Transmittance of the waveguides (t_w) was calculated considering losses along the different components involved in the whole system. Interface-waveguide transmittance ($t_{f-w} = 1 - \eta_R$), where η_R is the Fresnel reflection fibre guide, the mode-size mismatch between the fibre and the waveguide (η_0), interface transmittance (t_{out}) and microscope transmittance (t_m) are needed to be accounted in order to describe the overall throughput T, given by Eq. (8) [9].

$$T = t_{f-w}\eta_0 t_w t_{out} t_m \tag{8}$$

To determine the propagation losses (α_w), we use the extinction coefficient given by Eq. (9), where P_{in} and P_{out} are the input and output of optical power respectively and L is the waveguide length.

$$\alpha_w = -\ln\left(\frac{P_{in}}{P_{out}}\right)\Big/ L \tag{9}$$

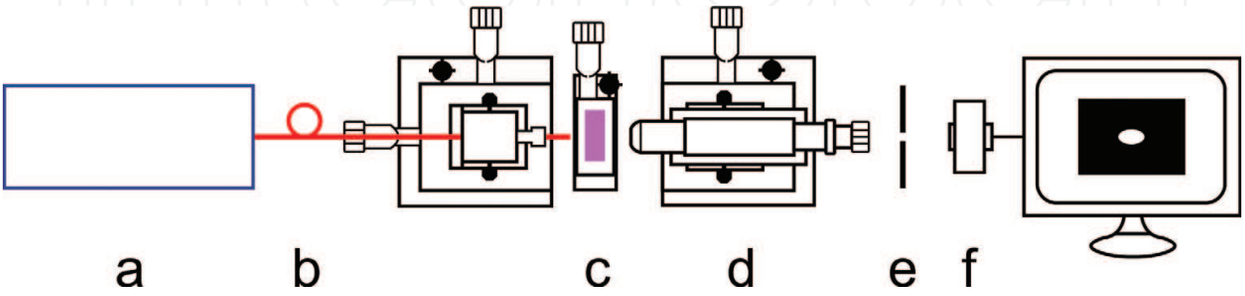

Figure 9. An experimental setup for a waveguide mode profile: (a) laser, (b) optical fibre, (c) waveguide, (d) microscope, (e) diaphragm and (f) CCD or detector.

http://dx.doi.org/10.5772/67829

To estimate losses and transmittance, power measurements were done by fibre-coupling into one waveguide facet, which introduces mainly three loss mechanisms: Fresnel reflections, size mismatch between the fibre mode and the waveguide mode and their misalignment [31].

The Fresnel reflection depends on the index change at both the waveguide and fibre end face. The reflected light (returned loss) can be written as:

$$\eta_R = \frac{\left(\frac{n_1-n_2}{n_1+n_2}\right)^2 + \left(\frac{n_3-n_2}{n_3+n_2}\right)^2 + 2\left(\frac{n_1-n_2}{n_1+n_2}\right)\left(\frac{n_3-n_2}{n_3+n_2}\right)\cos(4\pi n_2 g\frac{1}{\lambda})}{1+\left(\frac{n_1-n_2}{n_1+n_2}\right)^2\left(\frac{n_3-n_2}{n_3+n_2}\right)^2 + 2\left(\frac{n_1-n_2}{n_1+n_2}\right)\left(\frac{n_3-n_2}{n_3+n_2}\right)\cos(4\pi n_2 g\frac{1}{\lambda})} g \tag{10}$$

where n_1 and n_3 are the effective refractive indices of the fibre and the guide mode, n_2 is the refractive index in the gap g between the fibre and the guide and λ is the wavelength. The mode-size mismatch induces loss because the transverse mode coupling cannot be complete. The efficiency is computed using the well-known overlap integral

$$\eta_0 = \frac{\iint |E_1 E_2|^2 dxdy}{\iint |E_1|^2 dxdy \iint |E_2|^2 dxdy} . \tag{11}$$

This integral expresses the coupling between the electric fields E_1 and E_2 of modes, which propagates in the fibre and in the waveguide, respectively. In the most general case, the mode profile can be approximated by a combination of half Gaussians (see **Figure 10**) and the overlap integral gives:

$$\eta_0 = \frac{\left(\sqrt{\omega_1}\left(\frac{\omega_1}{\omega_0}+\frac{\omega_0}{\omega_1}\right)^{-1/2} + \sqrt{\omega_2}\left(\frac{\omega_2}{\omega_0}+\frac{\omega_0}{\omega_2}\right)^{-1/2}\right)^2}{\frac{\omega_1+\omega_2}{2}\left(\frac{\omega_3}{\omega_0}+\frac{\omega_0}{\omega_3}\right)} \tag{12}$$

where ω_0 is the waist of the fibre mode and ω_1, ω_2, and ω_3 are the half-waists of the waveguide mode. The propagation loss values (α_w) measured for the waveguides M_1, M_2 and M_4 are around 0.7, 3.9 and 19.5 dB/cm, respectively.

Figure 11 shows the intensity distribution of the propagation modes supported by the silver-implanted waveguides in SiO_2. These images of the spot emerging from the waveguide output, excited by fibre-waveguide coupling, were obtained by a Charge-coupled device (CCD) camera coupled to a travelling microscope. Here, it is possible to appreciate the excitation of propagation modes m_0 and m_1 for each of the waveguides, which is in accordance with results from the prism-coupling technique. The waveguide optical confinement factor measured for propagation modes m_0 and m_1 was 90% and 70% for M1, 80% and 75% for M2 and 90% and 85% for M4, respectively.

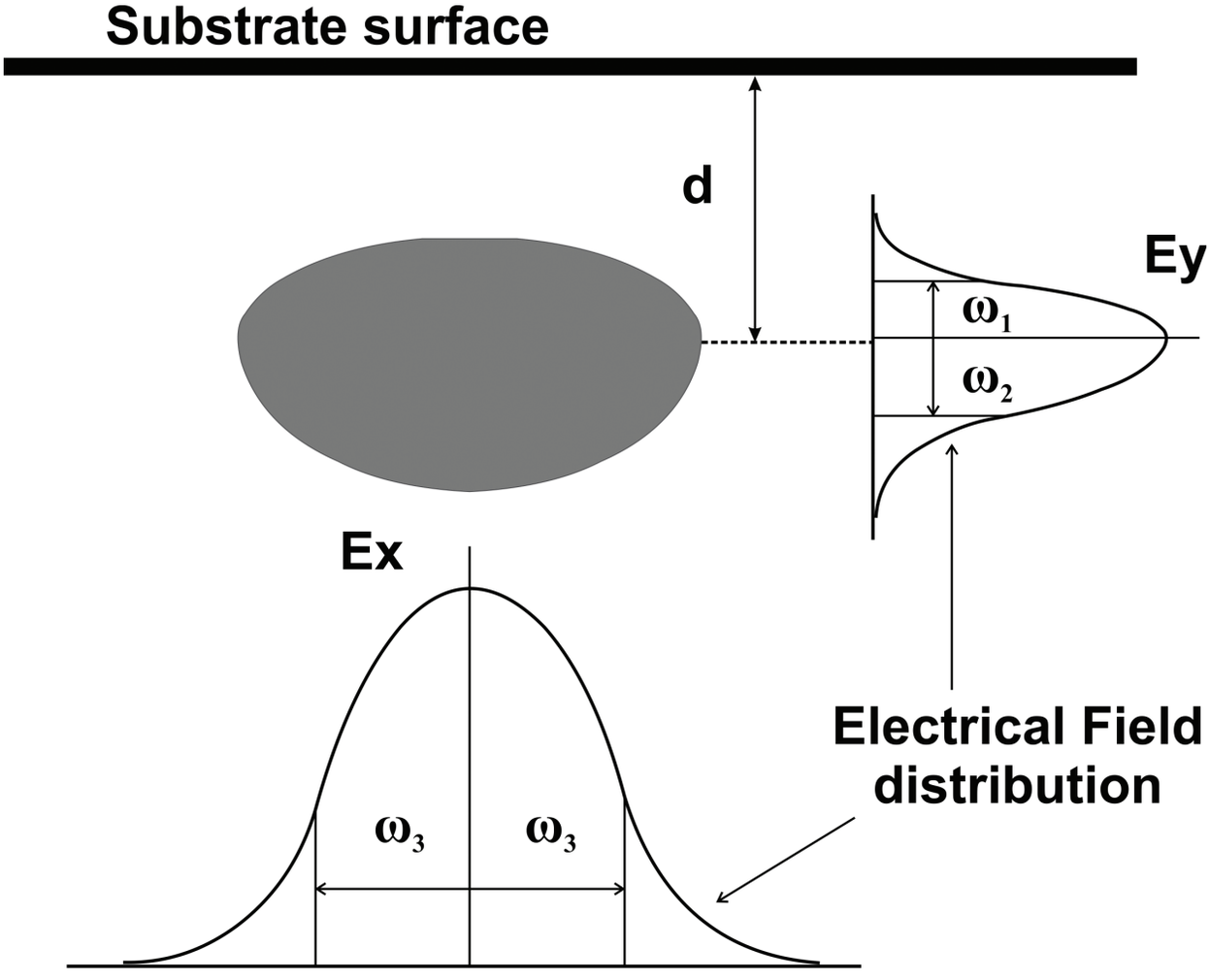

Figure 10. A typical waveguide mode profile [31].

4.4. Active optical waveguides

4.4.1. Laser emission

For more than 50 years, a large variety of lasers have been developed and optimized for different performance characteristics such as output power, efficiency, emission bands, pulse energy and pulse width. Research in this area is sustained by the impulse of a great diversity of scientific and technological applications in our modern society.

The main properties of laser emission are (a) coherence, which means that the photons move synchronously along the beam, (b) directionality, that is its ability to be focused into a small spot and (c) monochromaticity, which means that the light beam consists of essentially one wavelength, and this property originates from the basic principle of stimulated emission that involves well-defined atomic energy levels. Among different types of lasers, solid-state lasers are based on crystals or glasses doped with rare earth or transition metal ions. The principal source of energy to obtain efficient laser emission in these materials comes from laser diodes, giving solid-state lasers some advantages such as compact configuration, prolonged

http://dx.doi.org/10.5772/67829

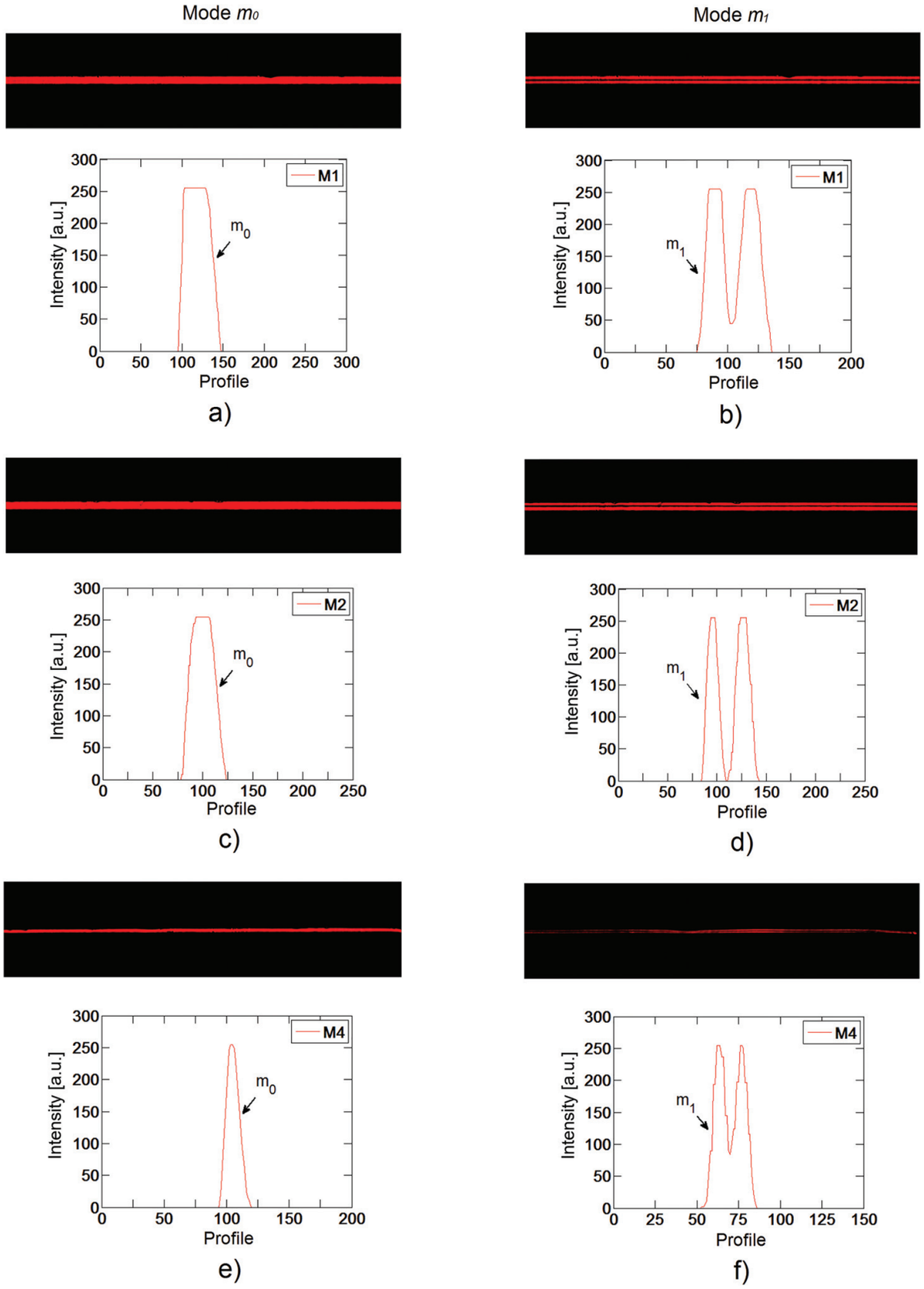

Figure 11. Intensity distributions of waveguide output light and intensity distribution profile for waveguides: a) fundamental mode in M1, b) first mode in M1, c) fundamental mode in M2, d) first mode in M2, e) fundamental mode in M4, and f) first mode in M4.

operational lifetime and generally very good beam quality. In particular, waveguide lasers offer high gain and low power thresholds in a small cross-section.

The principal laser characteristics are slope efficiency (ϕ) and threshold pump power (P_{th}); these are obtained from the plot of the laser output power as a function of the absorbed pump power (i.e., slope efficiency curve). The slope efficiency is the slope of the curve when it is approximated to a straight line, and the threshold pump power is the value of the pump power at which the curve crosses the pump power axis. For a four-level system like Nd:YAG or Nd:YVO_4, these parameters can be estimated using the following equations [32]:

$$\phi = \eta \frac{1 - R_2}{\delta} \frac{\lambda_p}{\lambda_s} \tag{13}$$

$$P_{th} = \frac{hc}{\lambda_p} \frac{1}{\eta \sigma_e \tau} \frac{\delta}{2} A_{eff} \tag{14}$$

where η is the pump quantum efficiency (number of ions excited to the upper-laser level per absorbed photon), $\delta = 2\alpha l - \ln(R_1 R_2)$ gives the total cavity losses (where α is the waveguide propagation loss and l is the cavity length), R_1 and R_2 are the reflectivities of the input and output mirrors, λ_p and λ_s are the pump and signal wavelengths, respectively, h is the Planck's constant, c is the speed of light in the vacuum, σ_e is the stimulated emission cross-section, τ is the fluorescence lifetime and A_{eff} is the effective pump area.

4.4.2. Optical waveguides in active crystals

Waveguides in laser and nonlinear crystals have been developed for several decades achieving a mature stage. In particular, rare earth-doped waveguides combine compactness and the possibility of generating laser light, by combining the absorption and emission properties of the active ion with the confinement capacity of the optical microstructure.

Numerous laser waveguides have been fabricated by ion implantation using the optical barrier approach (i.e., reducing the refractive index at some distance beneath the surface) [3–5]. In this case, multi-energy implantation has been used to broaden the barrier and thus reduce the light tunnelling into the substrate. Our group has reported laser waveguides in Nd:YAG, Yb:YAG and Nd:YVO_4 by light and heavy ion implantation [12, 27]. YAG waveguides exhibit a slight increase in the refractive index in the guiding region, besides the optical barrier, due to polarizability effects and optical stress. As an example of laser emission in these structures, channel waveguides fabricated by proton implantation in Nd:YAG showed a laser pump threshold of 6.9 mW and a slope efficiency of 16% [33], see **Figure 12**. Other groups have reported better laser performances (e.g., threshold pump power as low as 1.6 mW with a slope efficiency of 29%), indicating the improvement in the production of waveguide lasers [34].

Nd:YVO_4 waveguides have been fabricated by proton, helium, carbon and silicon implantation among different ions [26, 35, 36]. Implanting light ions generates the typical optical barrier waveguide for both the ordinary and the extraordinary index. We used double or triple implants to reduce the tunnelling losses. For example, a comparison was made between triple

http://dx.doi.org/10.5772/67829

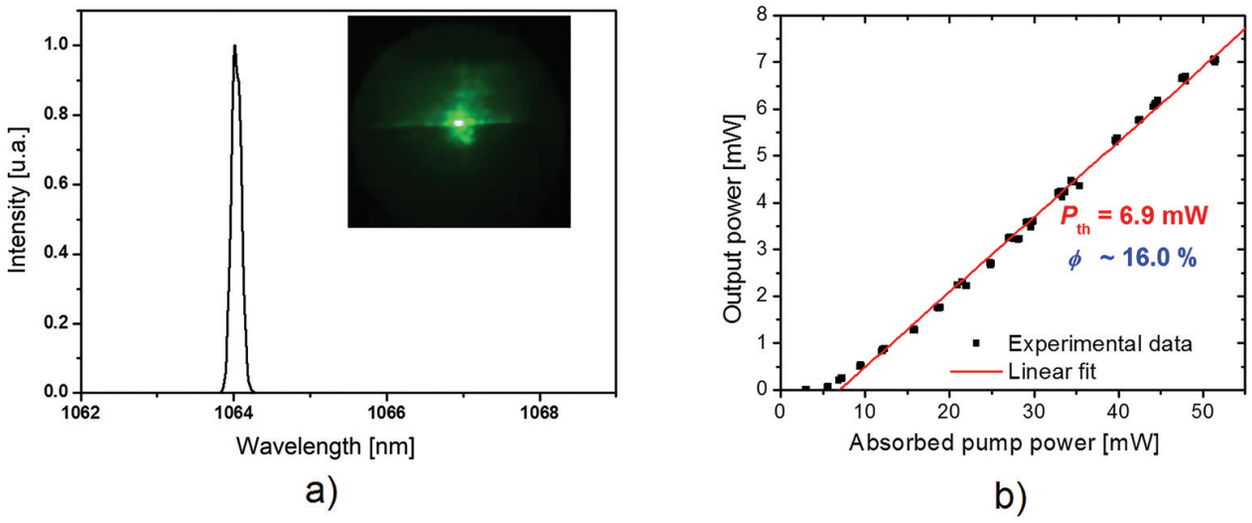

Figure 12. (a) Laser emission spectrum and (b) slope efficiency curve from a proton-implanted channel waveguide in Nd: YAG. The inset shows a photograph of the laser output at 1064 nm [33].

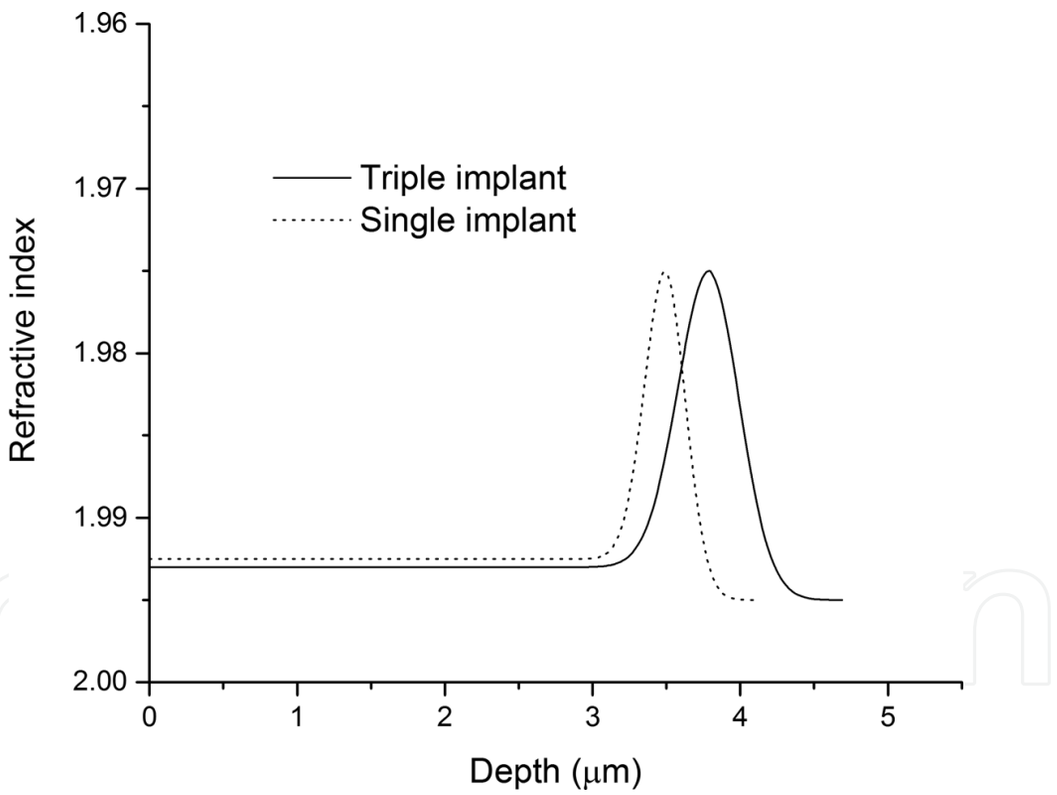

Figure 13. Refractive index profiles of Nd:YVO_4 waveguides implanted with a single implant and a triple helium implant [26].

helium-implanted and a single helium-implanted waveguide, see **Figure 13**; the light confinement was better in the multi-implanted waveguide due to the reduced tunnelling through the barrier. We also fabricated stacked waveguides in this crystal; in this case, we made two proton implants at 0.8 and 0.75 MeV to generate a deep broad optical barrier and a shallow implant at

0.4 MeV, thus producing a superficial and a buried waveguide. The buried waveguide had a better light confinement because the index contrast at the interface is smaller than in the shallow waveguide [26].

There are examples of materials that show a refractive index increase at certain light direction, thanks to their birefringence (e.g., YVO_4 and $LiNbO_3$). This property has been taken advantage in $LiNbO_3$ in order to produce a step-index profile for the extraordinary index by implanting carbon ions at 10 different energies [10]. However, it is possible to produce a refractive index increase with a single implant; this is realized by implanting heavy ions such as carbon and silicon at doses of around 10^{14} to 10^{15} ions/cm^2 [35, 36]. In this case, the refractive index profile exhibits an enhanced index well (i.e., the waveguide) and a region of reduced index at the end of the ion trajectory (i.e., the optical barrier). For a highly birefringent material, the electronic energy deposition causes lattice relaxation in the guiding region, increasing the lower index and reducing the higher one. We fabricated such waveguides (channels) in a Nd:YVO_4 crystal and demonstrated laser emission for the first time to our knowledge in a waveguide configuration. The threshold pump power was approximately 58 Mw, and the slope efficiency was around 24% [37].

4.5. Metallic nanoparticle-based optical waveguide

As it was previously described, ion implantation is a useful technique for producing waveguiding devices, either by using light ions to create a low index 'barrier' region or with metallic ions to increase the index in the implanted region and hence get guiding in this implanted region. On the other hand, it is well known that metal ions contained within a dielectric can be made to coalesce in order to form nanoparticles by thermal treatment in a reducing atmosphere [38]. The density and size of the nanoparticles can be controlled very well by controlling the implantation parameters such as dose and accelerating energy and by the thermal treatment parameters: temperature, duration and atmosphere composition. These nanocomposites containing metallic nanoparticles are very interesting from the point of view of their nonlinear optical properties, which are enhanced by the presence of localized surface plasmon resonance [39, 40].

The usual geometry for these samples is in the form of a thin layer, with thicknesses of the order of 1 μm, which are large enough to produce appreciable effects with low energy femtosecond pulses. It is therefore interesting to produce waveguides based on these metallic nanocomposite materials. The irradiance enhancement produced by the confinement of the electromagnetic field in a channel waveguide, and the considerably longer interaction length (from the mm to cm range), allows the observation of nonlinear effects with considerably smaller input pulse energies. Waveguide-based nonlinear devices are of particular interest for the implementation of ultrafast optical information processing applications [41] that exploit the nonlinear response to perform different functions. The fact that the region containing the metallic nanoparticles has a higher refractive index than the surrounding undoped silica substrate means that the implanted region can constitute the actual waveguide and that the nonlinear properties of the nanocomposite can be exploited for these applications, making them very good candidates for the implementation of such devices.

http://dx.doi.org/10.5772/67829

We have followed different approaches for the fabrication of channel waveguides containing metallic nanoparticles. In the first one, we have used a masked ion implantation to selectively implant Ag ions in narrow strips of the host, silica, followed by a thermal treatment to nucleate Ag nanoparticles [42]. As before, multiple implantations at different energies were employed to produce a cross-section that is large enough for efficient coupling by a single-mode fibre butt coupling. The energies employed in the successive implantations were 1.5, 2.0, 2.5, 3.0, 4.0 and 4.5 MeV. Because the widths and heights of the distribution vary with ion energy for a given dose, the doses at each energy were adjusted as to give the designed uniform profile. After the implantation process, the samples were thermally annealed at 600°C in a 50% N_2 + 50% H_2 reducing atmosphere for 1 hour, in order to obtain the highest amount of near-spherical nanoparticles by nucleation of the implanted ions. The end result is a sample containing channel waveguides with Ag nanoparticles, in a 2μm thick layer at a 0.52μm depth inside the silica matrix and having three different widths: 10,15 and 20 μm. **Figure 14** shows a white light microscope image of the waveguide and a front view of guided white light.

We characterized the linear optical properties of the waveguides produced using the techniques illustrated in **Figure 15(a)**. First, by looking at the light scattered perpendicular to the propagation direction, we can determine the propagation losses, and then by imaging the output at the guide end face, we can visualize the propagation modes of the guides. Propagation losses as low as 0.43 cm^{-1} were obtained for the 20 μm-wide guides using 633 nm light [42], and **Figure 15(b)** and **(c)** shows the measured modal field distribution, from where we can see that the guide supports three modes.

We have explored another approach for producing channel waveguides, which consists of direct writing of the waveguides by selective destruction of the nanoparticles using tightly

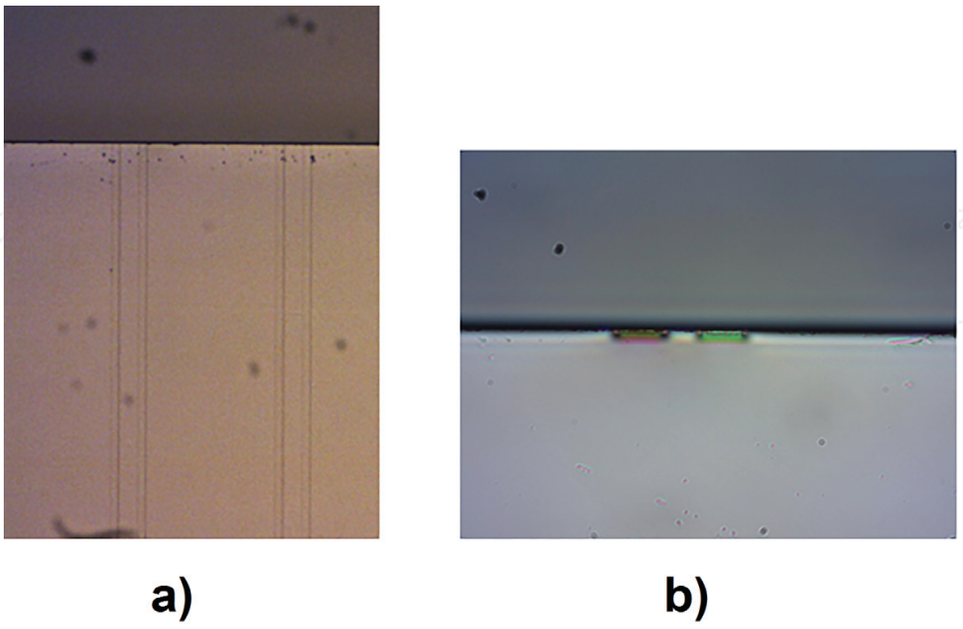

Figure 14. (a) A white light microscope image of an Ag nanoparticle waveguide (upper view) and (b) a front view of coupled white light output. The colouration is probably due to the plasmonic absorption of the nanoparticles.

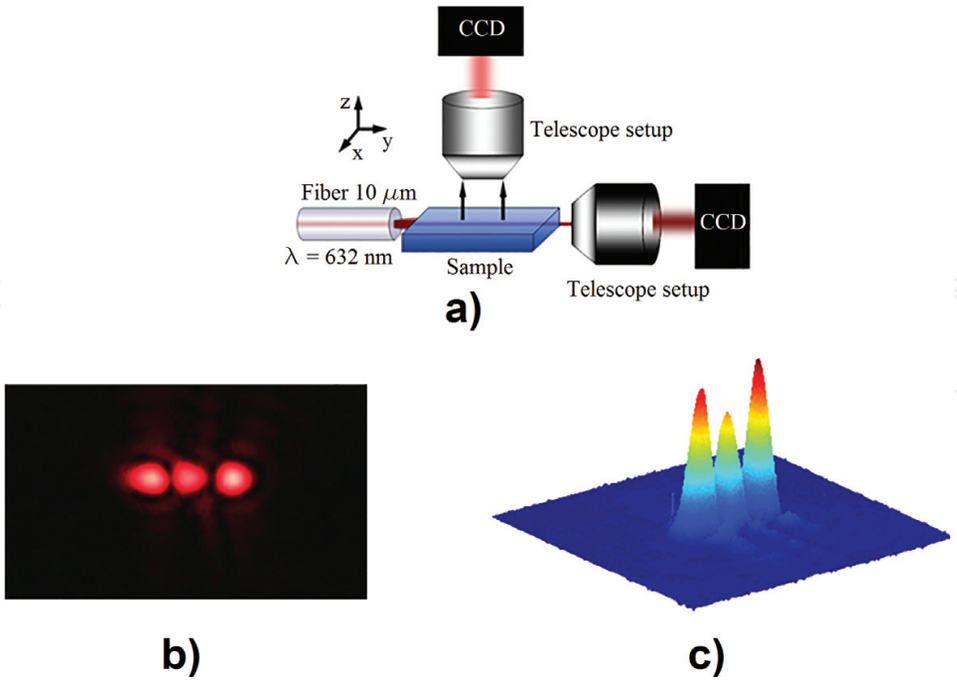

Figure 15. (a) An experimental set up to measure propagation losses and mode field distribution, (b) a 2D modal distribution measured for the 10 mm-wide guides and (c) an intensity plot for the measured mode.

focused *fs* pulses [43]. The advantage of this method is that by controlling the position of the laser pulses used, we can produce waveguides with different geometries and even more complex devices, such as Mach-Zehnder interferometers or directional couplers.

Based on our previous knowledge of the second harmonic generation properties of these materials [44], we employed a scanning second harmonic generation microscope based on an *fs* Titanium:sapphire laser oscillator, operated at high irradiances to produce the nanoparticle damage and at lower irradiances to image the damage achieved [43]. In this case, we used a sample that had elongated Ag nanoparticles that were aligned in a preferential direction, which was chosen to be at 45°C with respect to the sample surface [38]. This sample was chosen because of the relatively strong second harmonic signal observed [44] and the facility to induce damage. **Figure 16** shows a second harmonic image after we made two linear scans of the laser pulses at high intensity. It can be clearly seen that in the scanned regions, the second harmonic signal disappears almost completely, indicating the disappearance of the nanoparticles.

We have not observed waveguiding in these structures, but we expect to achieve it soon. This will allow us to produce different devices, such as beam splitters (Y junctions), Mach-Zehnder interferometers or directional couplers, which, together with the relatively large nonlinearities observed, can be used to implement all-optical switching devices, but of course, more work is needed in this direction.

Optical waveguides have been obtained through multiple energy ion implantations as a way to design optical waveguides with better optical confinement and lower propagation losses. The

http://dx.doi.org/10.5772/67829

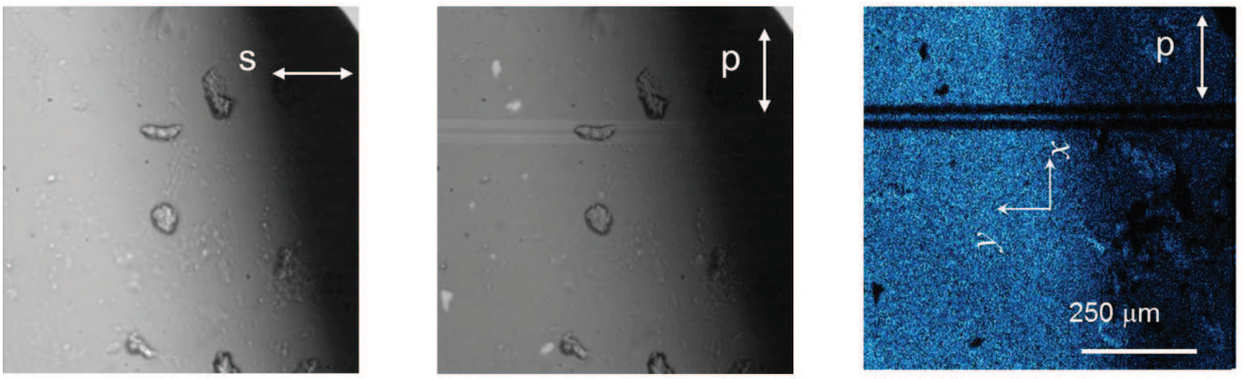

Figure 16. (a) Nanoparticle removal evidenced by the second harmonic generation and (b) white light microscopy images obtained with perpendicular polarizations, and (c) second harmonic image. Very high contrast is observed in the latter, indicating nanoparticle destruction.

protocol of design presented can be used with heavy ion implantation to enhance waveguide properties as core size and Δn; moreover, if the limit of metal solubility is reached, metallic nanoparticles can precipitate by means of annealing, bringing about a potential nonlinear optical waveguide. On the other hand, if light ions are used, it is possible to enhance the optical barrier or to design buried waveguides, that is, core waveguides formed between two barriers. This is possible due to the flexibility of the implantation process to change parameters as energy of implantation and fluence that must permit the development of active and passive integrated optical circuits.

5. Conclusions

Multiple ion implantation processes provide a potential way to produce optical waveguides using heavy and light ions, which improve capabilities to enhance optical confinement and reduce propagation losses—both paramount properties for optical waveguides. The protocol of design presented can be used with heavy ion implantation to enhance the core waveguide properties such as core size and Δn; moreover, if the limit of solubility of metal is reached, metallic nanoparticles can be produced by means of annealing, triggering a potential nonlinear optical waveguide. Ion implantation induces changes in polarizability, damage, compaction and stress that contribute directly to the refractive index profile and needs to be considered for advanced applications as active and passive integrated optical circuits.

Acknowledgements

The authors are grateful to CONACYT Grants No. 222485, No. J42695-F, No. 154021-F and DGAPA-UNAM IN-108217. The authors thank K. López and J.F. Jaimes for the IFUNAM Pelletron accelerator operation and Jessica Lilian Angel-Valenzuela for optical measurements support.

Author details

Heriberto Márquez Becerra[1]*, Gloria V. Vázquez[2], Eder G. Lizárraga-Medina[1], Raúl Rangel-Rojo[1] and David Salazar[1] and Alicia Oliver[3]

*Address all correspondence to: hmarquez@cicese.mx

1 Department of Optics, Center for Scientific Research and Higher Education at Ensenada, CICESE, Ensenada Baja California, México

2 Research Center in Optics, CIO, León Guanajuato, México

3 Institute of Physics, National Autonomous University of Mexico, UNAM, Mexico City, México

References

[1] Wang X, Ying C, Cao Z. Progress in planar optical (1st ed.). Berlin and Heidelberg: Springer-Verlag; 2016. 241 p. doi:10.1007/978-3-662-48984-0

[2] Schineller ER, Flam RP, Wilmot DW. Optical waveguides formed by proton irradiation of fused silica. J. Opt. Soc. Am. 1968;**58**(9):1171–1173

[3] Townsend PD, Chandler PJ, Zhang L. Optical effects of ion implantation (1st ed.). Cambridge: Cambridge University Press; 1994. 296 p

[4] Chen F, Wang X, Wang K. Development of ion implanted optical waveguides in optical materials: a review. Opt. Mater. 2007;**29(**11):1523–1542

[5] Chen F. Micro-and submicrometric waveguiding structures in optical crystals produced by ion beams for photonic applications. Laser Photon. Rev. 2012;**6**(5):622–640

[6] Liu CX, Peng B, Wei W, Li WN, Guo HT, Cheng S. Ion-implanted glass waveguides: a review. Phys. Int. 2013;**4**(1):1–12

[7] Tong XC. Advanced materials for integrated optical waveguides (1st ed.). Cham: Springer International Publishing; 2014. 552 p. doi: 10.1007/978-3-319-01550-7

[8] Xiang B, Ren X, Ruan S, Wang L, Yan P, Han H, Wang M, Yin J. Visible to near-infrared supercontinuum generation in yttrium orthosilicate bulk crystal and ion implanted planar waveguide. Sci. Rep. 2016;**6**:31612. doi:10.1038/srep31612

[9] Márquez H, Salazar D, Rangel-Rojo R, Angel-Valenzuela JL, Vázquez GV, Flores-Romero E, Rodríguez-Fernández L, Oliver A. Synthesis of optical waveguides by silver ion implantation. Opt. Mater. 2013;**35**(5):927–934

[10] Montanari GB, De Nicola P, Sugliani S, Menin A, Parini A, Nubile A, Bellanca G, Chiarini M, Bianconi M, Bentini GG. Step-index optical waveguide produced by multistep ion implantation in $LiNbO_3$. Opt. Express. 2012;**20**(4):4444–4453

[11] Ramabadran UB, Jackson HE, Boyd JT. Optical waveguides fabricated by ion implantation of Si^+, and N^+ in SiO_2: a Raman investigation. Appl. Opt. 1993;**32**(3):313–317

[12] Vazquez GV, Marquez H, Flores-Romero E, Sanchez-Morales ME. Optical waveguides fabricated by ion implantation in laser crystals. In: Espinoza-Luna R, Bernabeu E, Aboites V, editors. Recent research in photonics (1st ed.). Kerala: Research Signpost; 2009, pp. 153–181

[13] Ramírez-Espinoza C, Salazar D, Rangel-Rojo R, Angel-Valenzuela JL, Vázquez GV, Flores-Romero E, Rodríguez-Fernández L, Oliver A, Domínguez DA, Márquez H. Design of step-index optical waveguides by ion implantation. J. Lightwave Technol. 2015;**33** (14):3052–3059

[14] Lizarraga-Medina EG, Salazar D, Vázquez GV, Salas-Montiel R, Nedev N, Márquez H. Study of SiOx ($1 < \times < 2$) thin-film optical waveguides. J. Lightwave Technol. 2016;**34** (21):4926–4932

[15] Chen CL. Step-index thin film waveguides. In: Foundations for guided-wave optics (1st ed.). Hoboken: Wiley; 2007, pp. 25–49

[16] Wei DT, Lee WW, Blooom LR. Large refractive index change induced by ion implantation in lithium niobate. Appl. Phys. Lett. 1974;**25**(6):329–331

[17] Márquez H, Salazar D, Rangel-Rojo R, Angel JL, Vázquez GV, Flores-Romero E, Rodríguez-Fernández L, Oliver A. Waveguides by multiple implantations of Ag ion on SiO_2 substrates. In: Rodríguez-Vera R, Díaz-Uribe R, editors. 22nd Congress of the International Commission for Optics: Light for the Development of the World; October; Puebla. SPIE; 2011. doi:10.1117/12.901975

[18] Hernández-Mangas JM. Simulación de la implantación iónica en semiconductores [thesis]. Valladolid: Universidad de Valladolid; 2000, 192 p

[19] Biersack J.P., Haggmark L.G. A Monte Carlo computer program for the transport of energetic ions in amorphous targets. Nucl. Instr. and Meth. in Phys. Res. B. 1980;**174**(1–2): 257–269

[20] Ziegles J.F., Biersack J.P. The stopping and range of ions in matter. In: Bromley D.A., editor. Treatise on Heavy-Ion Science. New York: Springer US; 1985. p. 93–129. DOI: 10.1007/978-1-4615-8103-1_3

[21] Webb RP. Computer codes and simulation background to ion implantation distribution and sputtering programs. In: Briggs D, Seah MP, editors. Practical surface analysis: ion and neutral spectroscopy (2nd ed.). Hoboken: John Wiley & Son Ltd; 1992, pp. 657–704

[22] Posselt M. Crystal-trim and its application to investigations on channeling effects during ion implantation. Rad. Effects. 1994;**130**(1):87–119

[23] Ziegler J.F., Computer code SRIM. Available: http://www.srim.org in March 2017.

[24] Zhao JH, Du J, Wang FX, Qin XF, Fu G. Planar Nd:YGG waveguide fabrication by multiple energy He ion implantation. Nucl. Instrum. Meth. 2014;**326**:95–98

[25] Liu T, Liu P, Zhang L, Zhou YF, Yu XF, Wang XL. Planar waveguide in beta barium borate formed by proton implantation and optical properties in visible and near-infrared band. Opt. Mater. 2013;**35**(12):2068–2071

[26] Sánchez-Morales ME, Vázquez GV, Moretti P, Márquez H. Optical waveguides in Nd: YVO_4 crystals by multi-implants with protons and helium ions. Opt. Mater. 2007;**29** (7):840–844

[27] Vázquez GV, Ramírez D, Márquez H, Flores-Romero E, Rickards J, Trejo-Luna R. Waveguiding properties in Yb:YAG crystals implanted with protons and carbon ions. Appl. Opt. 2012;**51**(22):5573–5578

[28] Oven R. Polarizability, volume expansion, and stress contributions to the refractive index change of Cu^+-Na^+ ion exchanged waveguides in glass. Appl. Opt. 2011;**50**(26):5073–5079

[29] Najafi SI. Introduction to glass integrated optics (1st ed.). Norwood: Artech House Publishers; 1992, 180 p

[30] Chandler PJ, Lama FL. A new approach to the determination of planar waveguide profiles by means of a non-stationary mode index calculation. Opt. Acta. Int. J. Opt. 1986;**33** (2):127–143

[31] Bourhis J.F. Fiber-to-waveguide connection. In: S.I. Najafi, editor. Glass Integrated Optics and Optical Fiber Devices, Critical Reviews of Optical Science and Technology, SPIE Optical Engineering Press, CR53. San Diego, Ca., 1994, p. 335–366

[32] Clarkson WA, Hanna DC. Effects of transverse-mode profile on slope efficiency and relaxation oscillations in a longitudinally-pumped laser. J. Modern Opt. 1989;**36**(4):483–498

[33] Flores-Romero E, Vázquez, GV, Márquez H, Rangel-Rojo R, Rickards J, Trejo-Luna R. Laser emission in proton-implanted Nd:YAG channel waveguides. Opt Express. 2007;**15** (26):17874–17880

[34] Field SJ, Hanna DC, Large AC, Shepherd DP, Tropper AC, Chandler PJ, Townsend PD, Zhang L. Low threshold ion-implanted Nd:YAG channel waveguide laser. Electron. Lett. 1991;**27**(25):2375–2376

[35] Vázquez GV, Sánchez-Morales ME, Márquez H, Rickards J, Trejo-Luna R. Analysis of ion implanted waveguides formed on Nd:YVO_4 crystals. Opt. Commun. 2004;**240**(4–6): 351– 355

[36] Fu G, Wang KM, Wang XL, Lu F, Lu QM, Shen DY, Ma HJ, Nie R. Formation of planar optical waveguide by multi energy Si ion implantation into Nd:YVO_4 crystal. Surf. Coat. Technol. 2007;**201**(9–11):5427–5430

[37] Sánchez-Morales ME, Vázquez GV, Mejía EB, Márquez H, Rickards J, Trejo-Luna R. Laser emission in Nd:YVO_4 channel waveguides at 1064 nm. Appl. Phys. B. 2009;**94**(2):215–219

[38] Oliver A, Reyes-Esqueda JA, Cheang-Wong JC, Román-Velázquez CE, Crespo-Sosa A, Rodríguez-Fernández L, Seman JA, Noguez C. Controlled anisotropic deformation of Ag nanoparticles by Si ion irradiation. Phys. Rev. B. 2006;**74**(26):245425

[39] Hamanaka Y, Hayashi N, Nakamura A, Omi S. Dispersion of third-order nonlinear optical susceptibility of silver nanocrystal-glass composites. J. Lumin. 2000;**87**:859–861

[40] Rangel-Rojo R, McCarthy J, Bookey HT, Kar AK, Rodriguez-Fernandez L, Cheang-Wong JC, Crespo-Sosa A, Lopez-Suarez A, Oliver A, Rodriguez-Iglesias V, Silva-Pereyra H. Anisotropy in the nonlinear absorption of elongated silver nanoparticles in silica, probed by femtosecond pulses. Opt. Commun. 2009;**282**(9):1909–1912

[41] Paquot Y, Schröder J, Van-Erps J, Vo TD, Pelusi MD, Madden S, Luther-Davies B, Eggleton BJ. Single parameter optimization for simultaneous automatic compensation of multiple orders of dispersion for a 1.28 Tbaud signal. Opt. Express. 2011;**19**(25):25512–25520

[42] Can-Uc B, Rangel-Rojo R, Marquez H, Rodríguez-Fernández L, Oliver A. Nanoparticle containing channel waveguides produced by a multi-energy masked ion-implantation process. Opt. Express. 2015;**23**(3):3176–3185

[43] Licea-Rodríguez J, Rocha-Mendoza I, Rangel-Rojo R, Rodríguez-Fernández L, Oliver A. Femtosecond laser writing over silver nanoparticles system embedded in silica using nonlinear microscopy. Opt. Mater. 2014;**36**(3):682–686

[44] Rocha-Mendoza I, Rangel-Rojo R, Rodríguez-Fernández L, Oliver A. Second-order nonlinear response of composites containing aligned elongated silver nanoparticles. Opt. Express. 2011;**19**(22):21575–21587

IntechOpen